Published in final edited form as:

Stroke. 2023 June ; 54(6): 1593–1605. doi:10.1161/STROKEAHA.122.041853.

Rbpj deficiency disrupts vascular remodeling via abnormal Apelin and Cdc42 activity in brain arteriovenous malformation

Subhodip Adhicary, PhD[1,2], **Kayleigh Fanelli, MA**[1,3], **Sera Nakisli, BS**[1,3], **Brittney Ward, BS**[1,3,4], **Isaac Pearce, DO**[1,5], **Corinne M. Nielsen, PhD**[1,3,6,*]

[1]Department of Biological Sciences, Ohio University, Athens, OH, United States

[2]Translational Biomedical Sciences Program, Ohio University, Athens, OH

[3]Neuroscience Program, Ohio University, Athens, OH

[4]Honors Tutorial College, Ohio University, Athens, OH

[5]Heritage College of Osteopathic Medicine, Ohio University, Athens, OH

[6]Molecular and Cellular Biology Program, Ohio University, Athens, OH

Abstract

Background: Brain arteriovenous malformations (bAVM) are characterized by enlarged blood vessels, which direct blood through arteriovenous (AV) shunts, bypassing the artery-capillary-vein network and disrupting blood flow. Clinically, bAVM treatments are invasive and not routinely applicable. There is critical need to understand mechanisms of bAVM pathologies and develop pharmacological therapies.

Methods: We used an *in vivo* mouse model of Rbpj-mediated bAVM, which develops pathologies in the early postnatal period and an siRNA *in vitro* system to knockdown RBPJ in human brain microvascular endothelial cells (ECs). To understand molecular events regulated by endothelial Rbpj, we conducted RNA-Seq and ChIP-Seq analyses from isolated brain ECs.

Results: Rbpj-deficient (mutant) brain ECs acquired abnormally rounded shape (with no change to cell area), altered basement membrane dynamics, and increased EC density along AV shunts, compared to controls, suggesting impaired remodeling of neonatal brain vasculature. Consistent with impaired EC dynamics, we found increased Cdc42 activity in isolated mutant ECs, suggesting that Rbpj regulates small GTPase-mediated cellular functions in brain ECs. siRNA treated, *RBPJ*-deficient human brain ECs displayed increased Cdc42 activity, disrupted cell polarity and focal adhesion properties, and impaired migration *in vitro*. RNA-Seq analysis from isolated brain ECs identified differentially expressed genes in mutants, including *Apelin*, which encodes a ligand for G protein-coupled receptor signaling known to influence small GTPase activity. ChIP-Seq analysis revealed chromatin loci occupied by Rbpj in brain ECs that corresponded to G-protein and Apelin signaling molecules. *In vivo* administration of a competitive

*Correspondence author: Corinne M. Nielsen, PhD, Ohio University, Biological Sciences, 57 Oxbow Trail, Irvine 106, Athens, Ohio 45701, nielsenc@ohio.edu.

Disclosures

The authors declare no competing commercial or financial interests.

peptide antagonist against the Apelin receptor (Aplnr/Apj) attenuated Cdc42 activity and restored EC morphology and AV connection diameter in Rbpj-mutant brain vessels.

Conclusions: Our data suggest that endothelial Rbpj promotes rearrangement of brain ECs during cerebrovascular remodeling, through Apelin/Apj-mediated small GTPase activity, and prevents bAVM. By inhibiting Apelin/Apj signaling *in vivo*, we demonstrated pharmacological prevention of Rbpj mediated bAVM.

Graphical Abstract

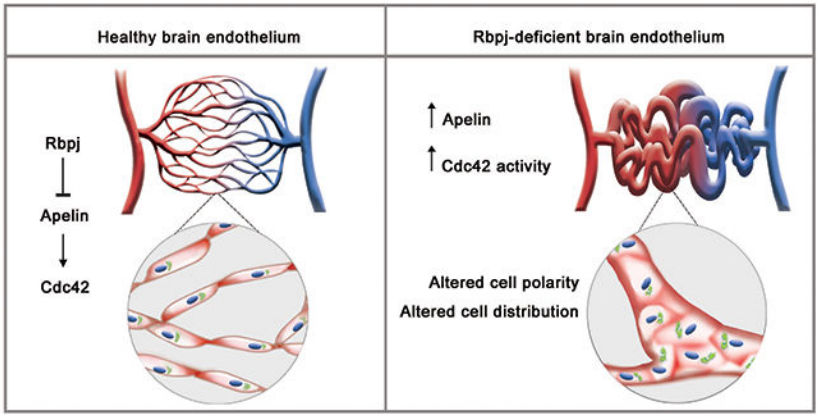

Keywords

Apelin; brain arteriovenous malformation; Cdc42; GTPase; Rbpj

Introduction

Brain arteriovenous malformation (bAVM) is a neurovascular disease characterized by enlarged, tortuous vessels and AV shunting, which connects arteries directly to veins and may lead to tissue hypoxia, stroke, and neurological deficit. Treatments for bAVM are limited, but as disease mechanisms are uncovered, new prevention and treatment strategies can be developed.

Recombination signal-binding protein for immunoglobulin Jκ regions (Rbpj) is a transcriptional regulator of Notch signaling, which is critical for vascular endothelial homeostasis during different stages of mammalian life.[1,2] Recent studies described Notch-independent roles for Rbpj, during cardiac angiogenesis and neurovascular pericyte maintenance.[3,4] Perturbations to Notch signaling molecules lead to bAVM formation in mice[5,6], and misexpression of Notch signaling factors has been reported in TGF-β associated models of bAVM.[7,8] Human bAVM tissue samples show misexpression of NOTCH receptors, ligands, and downstream effectors.[9–11] Genomic studies have revealed *NOTCH4* polymorphisms as associative risk factors for bAVM and hemorrhage[12], supporting Notch's association with human bAVM.

Small guanosine triphosphate (GTP)-ases (e.g., Rho, Rac, and Cdc42), belong to a superfamily of molecules that regulate gene expression, cell adhesion, directed migration,

and cytoskeletal properties[13], and are regulated by guanine nucleotide exchange factors (GEFs), GTPase activator proteins (GAPs), and guanosine nucleotide dissociation inhibitors (GDIs). Apelin is a regulatory peptide that signals via a G protein-coupled receptor (GPCR) – Apelin receptor (Aplnr/Apj). Apelin signaling has regulatory roles in vascular endothelium, including regulation of EC polarization and vessel caliber size and rearrangement of ECs along vessels in zebrafish.[14]

Here, using an Rbpj-deficient bAVM mouse model that develops AV shunts by P14[6] and an *in vitro* human brain EC culture system, we uncovered roles for endothelial Rbpj to promote neurovascular modeling and prevent bAVM pathogenesis, via regulation of Apelin and Cdc42.

Methods

Detailed methods in Supplemental Material. Data were acquired/reported following ARRIVE guidelines[15] (Table S1). The data that support the findings of this study are available from the corresponding author upon reasonable request. RNA-Seq and ChIP-Seq data are available as GEO subseries GSE223531 and GSE223532, respectively.

Mice and tissue harvest

Experimental mice and tissue harvest were previously described.[6] Experiments were approved by Ohio University Institutional Animal Care and Use Committee Protocol #16-H-024.

Quantification of AV connection diameter and EC shape

Acquisition of AV connection measurements have been previously described.[6] Area, length, width measurements for Cadherin5(+) ECs from whole-mount cerebrovasculature were made with NIS-Elements.

Immunolabeling

Whole-mount (WM) and section immunostaining used blocking reagent (5% donkey serum, 0.1% PBS-Triton X-100); primary and secondary antibodies listed in Table S2. DAB substrate (ThermoFisher) was used for paraffin sections.

EdU incorporation and TUNEL

Click-iT EdU AlexaFluor 647 Imaging Kit (Invitrogen) and Click-iT TUNEL Alexa Fluor 647 Imaging Kit (Invitrogen) was used following manufacturer’s instructions.

Endothelial cell sorting

Tissue was minced/digested with DMEM/5% heat-inactivated fetal bovine serum/700 U/ml collagenase II (Worthington)/2.4 U/ml neutral protease (Worthington)/140 U/ml DNase I (Worthington). Suspension was centrifuged through 70% Percoll (GE Healthcare) gradient. Cells were sorted on BD FACSAria Cell Sorter (FACSDiva software, BD Bioscience, Version 6.0) or with CD31 magnetic microbeads/MACS columns (Miltenyi).

RNA extraction and qPCR

Total RNA was extracted using RNeasy Plus Micro Kit (Qiagen); qPCR was performed with qScript One-step qPCR kit (QuantaBio). Primers listed in Table S3.

RNA sequencing

Paired-ended Poly(A) RNA sequencing was performed on a NovaSeq 6000 platform. Reads were mapped to the *Mus musculus* GRCm39 Ensembl release 96 genome. FPKM values were calculated from compiled transcriptome. Differentially expressed mRNAs were selected with $\log_2$ (fold change) > 1 or $\log_2$ (fold change) < −1 and with statistical significance (P value < 0.05) using edgeR.

siRNA transfection

Human cerebral microvascular hCMEC/D3 cells (Millipore) were transfected with Lipofectamine RNAiMAX Transfection Reagent (ThermoFisher) and Silencer-Select (Ambion) siRNA (siRNA assay ID#s223924) complex, targeted against *RBPJ* (NM_203284.2).

Western blotting

Western blotting followed standard procedures with PVDF membranes immunoblotted against Rabbit anti-RBPJ (1:1000, Cell Signaling, #5313) and Rabbit anti-GAPDH (1:1000, Cell Signaling Technology, #5174).

Migration and Immunolabeling in hCMEC/D3 cells

Assay was performed in migration chambers (iBidi) with 500 μm culture insert. Cells were imaged under brightfield optics after the removal of physical insert (t_0) and 12 hrs post-migration (t_{12}). Cell-free area was determined using Wound healing plugin (Wound_healing_size_tool.ijm) on ImageJ software (NIH, Rockville, MD, USA). Cells were immunolabelled using rabbit anti-GM130 (Invitrogen, #PA5-95727, 1:800), Acti-stain™ 555 Fluorescent Phalloidin (Cytoskeleton Inc., #PHDH1, 1:500), rabbit anti-Phospho-Paxillin (Tyr118) (Invitrogen #44-722G, 1:500).

Front-rear polarity analysis in hCMEC/D3 cells

A cell was considered polarized towards direction of migration when Golgi apparatus oriented within ± 45 ° perpendicular to cell free gap. Rose plot was constructed using GeoRose software (V0.5.0, Yonggeng Ye, Alberta, Canada).

GTPase activity

Activity of small GTPases were evaluated using G-LISA Activation Assay (Cytoskeleton Inc.), according to manufacturer's instructions.

In vivo vascular permeability

AlexaFluor™ 647 conjugated 10,000 molecular weight (MW) dextran (ThermoFisher, 200 μg) and heparin (5 Units/10 g body weight, Alfa Aesar) were injected via inferior vena cava.

20 μm sagittal sections were imaged. Mice were intraperitoneally injected with 2% Evans blue in 0.9% sterile saline solution. 1 mm brain slices were imaged using fluorescent and brightfield microscopy (Nikon Eclipse-NiU).

In vivo Apj antagonism

Rbpj$^{i\Delta EC}$ were injected intraperitoneally with Cyclo(1-6)CRPRLC-KH-Cyclo(9-14)CRPRLC, (Phoenix Pharmaceuticals) at 2 μg/mg body weight, at P7, P10, P12. Vehicle control Rbpj$^{i\Delta EC}$ mice received sterile PBS injections with identical volumes. P14 brains were harvested for experimental analyses.

Chromatin immunoprecipitation (ChIP)

ChIP was performed against Rbpj (Cell Signaling 1:50, #5313) from isolated P7 FVB/NJ mice (Jackson Laboratories 001800) brain ECs. Libraries were prepared using NEBNext Ultra II DNA Library Prep Kit with 2 ng of immunoprecipitated DNA and 2% input samples, followed by paired-end sequencing on NovaSeq 6000 platform. Reads were aligned to *Mus musculus* reference: mm10. Peak detection was achieved using MACS2 and visualized via IGV (V2.13.2). Primers listed in Table S4.

Confocal imaging

Z-stack images were acquired on Zeiss LSM 510 laser scanning confocal microscope, with ZEN Software 2.3 (Carl Zeiss), and projected at maximum intensity.

Statistical analysis

Statistical tests used: Shapiro-Wilk, Kolmogorov-Smirnov, unpaired *t*-test with Welch's correction, one-way ANOVA, Tukey's multiple comparison, Mann Whitney, two-tailed, one-sample Student's *t* test. Error bars indicate standard deviation, unless stated otherwise. Statistical significance was reported as *p<0.05, **p<0.01, ***p<0.001, ****p<0.0001, using GraphPad Prism (Version 9.3.1). Power analyses for all experimental datasets are reported in Table S5.

Results

Rbpj was absent from Rbpj$^{i\Delta EC}$ brain ECs by P7, but AV microvessel diameter remained unchanged

We first defined the timing of early postnatal bAVM initiation and progression. While Rbpj deletion was verified in brain tissues at P14[6,16], and from isolated brain ECs at P7[17], we wanted to identify a timepoint at which Rbpj was absent from ECs, but at which features of bAVM had not developed, to circumvent confounding effects of established pathologies. We bred *Cdh5(PAC)-CreER^{T2}; Rbpj$^{flox/WT}$* (control) and *Cdh5(PAC)-CreER^{T2}; Rbpj$^{flox/flox}$* (Rbpj$^{i\Delta EC}$ mutant) mice and induced endothelial Rbpj deletion at P1 and P2. Because Rbpj$^{i\Delta EC}$ mice develop features of bAVM and 50% lethality by P14[6], we quantified the abundance of enlarged AV connections at P14. In frontal cortex and cerebellum (combined measurements from both brain regions), all control AV connections had diameters in the capillary range (<6 to ≤8 um). For Rbpj$^{i\Delta EC}$ AV connections, approximately 15/90 (16.7%)

had diameters in the capillary range (<6 to ≤8 um), while 75/90 (83.3%) had diameters in abnormally enlarged ranges (>8 to <12.5um and ≥12.5 um) (Figure S1). Next, we selected P5, P7, and P10 as timepoints for analyses. By P5, Rbpj knockdown in Rbpj$^{i\Delta EC}$ mice was inconsistent (Figure S2), but by P7, Rbpj protein was absent from Rbpj$^{i\Delta EC}$ ECs (Figure S3B–C) and brain AV connection diameters were not changed between control and Rbpj$^{i\Delta EC}$ (Figure S3D, quantified in E). By P10, brain AV connection diameters were increased in Rbpj$^{i\Delta EC}$ mice as compared to controls (Figure S3E). Thus, we studied P7 (bAVM initiation), P10 (moderate bAVM pathology) and P14 (advanced bAVM) as stages to uncover cellular and molecular events involved in bAVM formation and progression (Figure S3A).

Endothelial Rbpj-deficient brain microvessels exhibited abnormal EC morphology, increased EC density, and decreased empty basement membrane sleeves

We investigated whether Rbpj$^{i\Delta EC}$ shunts formed by increased EC proliferation or decreased EC apoptosis. We analyzed EdU incorporation from P5-7 and from P12-14 (Figure S4A) and found no difference in the number of double-positive EdU(+)/lectin(+) ECs per area of brain tissue and between control and Rbpj$^{i\Delta EC}$ tissue at P5-7 or P12-14 (Figure S4B–C). We analyzed apoptosis at P7 and P14 and found no difference between the number of double-positive TUNEL(+)/lectin(+) ECs per area of brain tissue control and Rbpj$^{i\Delta EC}$ tissue at P7 or P14 (Figure S4D–E). These results indicate that neither proliferation nor apoptosis contributed to Rbpj$^{i\Delta EC}$ AV shunting.

To examine EC hypertrophy, we traced Cadherin5(+) EC membranes, then measured the outlined cellular areas (Figure 1A). We found no difference in P7 or P14 brain EC area in Rbpj$^{i\Delta EC}$ mice, as compared to controls (Figure 1B), suggesting that EC hypertrophy did not contribute to AV shunting in Rbpj$^{i\Delta EC}$ mice. We examined EC morphology by measuring cell shape index (EC length/EC width) in P7, P10 and P14 mice. We found that ECs comprising Rbpj$^{i\Delta EC}$ AV shunts were abnormally rounded or ellipsoid by P14 (Figure 1A), with a length-width index significantly lower than that of elongated ECs in control capillaries (Figure 1B). Because abnormally shaped brain ECs gave the appearance of increased EC density, we counted the number of ECs on AV connections <12.5 μm and on those ≥12.5 μm (operational definition for AV shunts in Rbpj$^{i\Delta EC}$ mice[18]). At P14, we found increased cell density per vessel length in Rbpj$^{i\Delta EC}$ AV shunts, as compared to healthy Rbpj$^{i\Delta EC}$ AV connections (Figure 1B). To understand cellular dynamics over time, we found that EC shape index increased from P7 to P14 in controls (Figure 1C) but not in mutants (Figure 1C). These data indicate that in control, early postnatal brain, ECs elongated over time, and a primitive vascular plexus refined into capillary-like vessels. In Rbpj$^{i\Delta EC}$ mutants, we found no change to EC shape index from P7 to P14 (Figure 1C) and increased cell density from P7 to P14 (Figure 1C). These data suggest that in Rbpj$^{i\Delta EC}$ brain vasculature, EC elongation and refinement into capillary-like vessels was impaired.

To test whether cerebrovascular refinement was affected, we counted empty basement membrane sleeves (EBMS) – empty vessel sleeves whose ECs have rearranged or migrated away.[19] We first assessed the number of Collagen IV(+)/Cadherin5(−) EBMS in P7 brain vasculature (Figure 1D), reasoning that Rbpj$^{i\Delta EC}$ impaired microvessel regression would manifest pre-shunting. We found reduced EBMS per brain area in Rbpj$^{i\Delta EC}$, as compared to

controls (Figure 1E). In control tissue, EBMS decreased over time, from P7 to P14, while in Rbpj$^{i\Delta EC}$ tissue, EBMS did not change (Figure 1E), suggesting that brain vessel regression was perturbed. Our findings suggest that endothelial deletion of Rbpj disrupts early postnatal cerebrovascular remodeling, perhaps by a lack of EC redistribution and rearrangement along AV connections.

Endothelial *RBPJ* deficiency in human microvascular brain ECs perturbed cell migration, directionality, and polarity, with altered focal adhesion properties

To study endothelial Rbpj roles independent of blood flow, we knocked down *RBPJ* in human cerebral microvascular ECs (hCMEC/D3 cells) and confirmed RBPJ knockdown (si*RBPJ*), compared to scrambled controls (si*Scr*) (Figure S5A–B). To test whether RBPJ deficiency affects directed EC movement, we performed a migration assay. From time $(t)_0$ hrs to t_{12} hrs, both wild-type and si*Scr* cells moved toward the acellular gap and covered the area to a greater degree than si*RBPJ* cells (Figure 2A), suggesting that endothelial RBPJ is required for directed brain microvascular EC movement.

Because front-rear polarity is required for directed cell movement, we tested cell polarization, following t_{12} hrs of migration. Using the position of the intracellular Golgi apparatus, relative to the cell nucleus (Golgi are positioned at the ‘leading edge’ of a migrating cell), we found impaired cell polarization in si*RBPJ* cells, as compared to si*Scr* (Figure 2B). We constructed Rose plots that depict the degree of polarization (polarized = ± 45 ° perpendicular to the acellular gap; non-polarized = greater than ± 45 ° perpendicular) and the number of cells within specific degree ranges (Figure 2C). The average angle of polarization and percentage of non-polarized cells were greater for si*RBPJ* cells, compared to si*Scr* (Figure 2D–E). These data suggest that endothelial RBPJ regulates cell polarization in brain microvascular ECs.

We hypothesized that altered focal adhesion (FA) assemblies would be associated with impaired cell migration in si*RBPJ* cells. We found increased number of actively remodeling, phosphorylated-Paxillin (p-Y118 Pax)(+) FAs per cell in si*RBPJ* cells, as compared to si*Scr* (Figure 2F). This suggests that RBPJ participates in FA assembly, which subsequently influences cell adhesion and migration properties.

Endothelial deletion of Rbpj led to dysregulated GAP/GEF expression, small GTPase activity, and vascular permeability

We tested activity of small GTPases (Rho subfamily) and found increased Cdc42 activity in si*RBPJ* cells, compared to si*Scr*, and in P7 and P14 Rbpj$^{i\Delta EC}$ brain ECs, compared to controls (Figure 3A). By contrast, RHOA and RAC1 activities were not altered in si*RBPJ* cells, compared to si*Scr* (Figure S6A–B), and were decreased in P7 Rbpj$^{i\Delta EC}$ brain ECs, compared to controls (Figure 3B–C). Next, we found that expression of *ARHGAP18*, *ARHGAP29*, and *DOCK6* was increased, and expression of *ARHGAP21* was decreased, in si*RBPJ* cells, as compared to si*Scr* (Figure 3D). In P7 mouse brain ECs, expression of *Arhgap18*, *Arhgap21*, *Arhgap29*, and *Dock6* increased in Rbpj$^{i\Delta EC}$, as compared to controls (Figure 3D). At P14, increased expression of *Arhgap18*, *Arhgap29*, and *Dock6* was sustained, while expression of *Arhgap21* was decreased (Figure 3D). Together, these

data suggest that (i) in mammals, endothelial Rbpj/RBPJ-mediated regulation of Cdc42 is conserved, but regulation of GAPs, GEFs, and other GTPases differs, (ii) RBPJ regulates GAPs, GEFs, and CDC42 activity independent of *in vivo* physiological influences, and (iii) small GTPases contribute differentially to morphogenesis of early postnatal mouse brain vasculature.

Because small GTPase activity is linked to changes in vessel permeability[20], we hypothesized that Rbpj$^{i\Delta EC}$ brain vessels would have increased permeability. We intravenously or intraperitoneally injected 10 kDA dextran or 67 kDa Evans blue, respectively, into P14 mice and found extravasated dextran (Figure 3E) and Evans blue (Figure S7) in brain parenchyma of Rbpj$^{i\Delta EC}$ mice, but not controls. We found robust expression of Claudin-5, a blood-brain barrier tight junctional protein, in control and Rbpj$^{i\Delta EC}$ brain ECs at P15 (Figure S8A–C). In whole-mount cortex, we found Claudin-5 expressed by ECs in capillaries (control) and AV shunts (Rbpj$^{i\Delta EC}$) (Figure S8D). We used high-resolution imaging to show that Claudin-5 was transported to EC membranes in control and mutant brain tissue (Figure S9A–B). We examined ZO-1, another tight junctional protein, and found robust expression in P14 brain ECs from control and Rbpj$^{i\Delta EC}$ mice (Figure S10A–B). Our data suggest that endothelial Rbpj is not required for expression of tight junctional proteins Claudin-5 and ZO-1.

RNA sequencing identified differentially expressed genes in isolated P7 brain ECs, following endothelial deletion of Rbpj

To understand how Rbpj deficiency affects gene expression during bAVM initiation, we performed transcriptome analysis via bulk RNA-Seq (GEO subseries GSE223531). Sequencing results revealed differentially expressed genes (DEGs) in brain ECs – 273 upregulated and 164 downregulated genes in P7 Rbpj$^{i\Delta EC}$ mice, as compared to controls, indicating roles for Rbpj as a transcriptional repressor and activator, respectively (Figure 4A). Identification of *Rbpj* within the downregulated group confirmed allele deletion, and presence of capillary-specific genes within the solute carrier family (*Slco1a4*) validated ECs form AV connections. Comprehensive gene ontology (GO) enrichment analysis (Figure 4B) revealed genes encoding membrane localized, protein and ion interacting, and cell adhesion regulating molecules. Kyoto Encyclopedia of Genes and Genome (KEGG) pathway enrichment analysis (Figure 4C) displayed similar results, with enriched genes encoding molecules involved in extracellular matrix-receptor, ligand-receptor interactions, and focal adhesion regulation, suggesting roles for endothelial Rbpj in regulating cellular signaling.

We selected DEGs of interest by screening for expression changes between control and Rbpj$^{i\Delta EC}$ brain ECs (Figure 4D) and for fragments per kilobase of transcript per million fragments mapped (FPKM) values (Figure S11). DEG expression was validated with an independent cohort of flow-sorted brain ECs from control and Rbpj$^{i\Delta EC}$ mice. Expression of *Rbpj* and *Efnb2* was decreased in Rbpj$^{i\Delta EC}$ ECs, which confirmed endothelial *Rbpj* deletion (Figure 4E). Among upregulated genes of interest, *Adrenomedullin* (*Adm*), *Secreted phosphoprotein 1* (*Spp1*, encoding Osteopontin), and *Apelin* (*Apln*) were selected for further analysis. Increased expression of *Adm*, *Spp1*, and *Apln* was sustained in Rbpj$^{i\Delta EC}$ versus

control ECs at P10 and P14 (Figure 4F) and in si*RBPJ* D3 cells, as compared to si*Scr* (Figure S5A), suggesting an evolutionarily conserved role for endothelial Rbpj to regulate *Adm*, *Spp1*, and *Apln* expression, independent of physiological influences. These results suggest that endothelial Rbpj is required to mediate downstream gene expression in the early postnatal brain vasculature to prevent bAVM pathologies.

ChIP-Seq identified Rbpj occupancy signature in isolated P7 brain ECs, including molecules involved in Apelin signaling and in regulating small GTPase activity

To map chromatin regions occupied by Rbpj in an early postnatal cerebrovasculature, we conducted a Chromatin Immunoprecipitation Sequencing (ChIP-Seq) experiment (GEO subseries GSE223532). Genomic distribution of Rbpj-binding peaks revealed most sites being intergenic (38%) or intronic (36%) and others within promoter, 5'UTR, or −2 kb of transcriptional start sites (5% collectively) (Figure 5A), Thirteen GAPs or GEFs were identified as Rbpj binding targets (Table S6), and 17 genes identified as DEGs in our RNA-Seq dataset overlapped with Rbpj ChIP-Seq data (Figure 5B and Table S6). The intersectional cohort included *Arhgap20*, *Arhgef28*, *Adm*, *Akt3*, and members of the *Protocadherin* gene family (*Pcdhga4-10*). Other loci of interest included regions around genes encoding solute carriers, *Hdac9*, and *EphB1* (Figure S12A–E; Table S6). These data suggest that Rbpj directly regulates select GAPs and GEFs in P7 brain ECs, consistent with our data showing that endothelial Rbpj regulates small GTPase activity in brain ECs.

GO enrichment analysis (Figure 5C) revealed genes that encode membrane-localized signaling molecules, involved in GTPase activator and kinase activity, and the cytoskeleton, similar to RNA-Seq analysis. KEGG analysis (Figure 5D) displayed enriched genes involved in GTPase signaling, cAMP signaling, cell adhesion, and Apelin signaling. Targets involved in Notch signaling were identified and enriched in KEGG analysis (Figure 5D), including Rbpj binding target *Hairy and enhancer of split-1* (*Hes1*) (Figure 5E). We observed enrichment peaks for genomic regions for Apelin-related genes: *G-protein subunit alpha i1* (*Gnai*) encodes a protein that is coupled to Aplnr/Apj[21]; *Guanine nucleotide-binding protein G(q) subunit alpha* (*Gnaq*) encodes a protein involved in GPCR signaling, and human GNAQ mutations were implicated in vascular malformations[22]; *Myocyte enhancer factor 2C* (*Mef2c*) is regulated by Apelin signaling in cardiovascular development[23] (Figure 5E). These data support the hypothesis that Rbpj directly regulates Apelin signaling and small GTPase activity in cerebrovascular ECs.

Pharmacological blockade of Apelin/Apj signaling restored brain AV connection diameter, EC shape index, and Cdc42 activity in Rbpj$^{i\Delta EC}$ mice

Given that (i) Apelin expression was increased in Rbpj-deficient brain ECs (Figure 4), (ii) Apelin receptor is coupled to Gnai1[21], (iii) Apelin has been shown to regulate EC signaling[24], (iv) Apelin signaling molecules and GPCR subunits were identified as direct Rbpj transcriptional targets (Figure 5), we hypothesized that endothelial Rbpj negatively regulates Apelin signaling to maintain healthy cerebrovascular remodeling and prevent AVM formation. We used a small peptide antagonist (MM54 (Cyclo(1-6)CRPRLC-KH-Cyclo(9-14)CRPRLC), targeted against the Apelin receptor (Apj), to test whether inhibition of Apelin signaling prevents bAVM formation in Rbpj$^{i\Delta EC}$ mice (Figure 6A). Administration

of the Apj antagonist in Rbpj$^{i\Delta EC}$ mice ameliorated vessel diameter enlargement (Figure 6B, quantified in D) and EC shape index change (Figure 6C, quantified in D), prevented the increase in Cdc42 activity (Figure 6D), and attenuated 10 kDa Dextran extravasation (Figure 6D–E), as compared to vehicle-treated Rbpj$^{i\Delta EC}$ mice. These findings suggest that endothelial Rbpj mediates Apelin signaling and regulates downstream activation of Cdc42, to inhibit vessel permeability in early postnatal brain vasculature.

Discussion

Our data indicate a critical role for endothelial Rbpj to govern reorganization of the primitive cerebrovascular plexus, via regulation of Apelin signaling and Cdc42 activity, thereby preventing AV shunting in the early postnatal brain. Rbpj$^{i\Delta EC}$ ECs underwent morphological changes, without evidence for hypertrophy or hyperplasia, contrasting cellular changes found in other bAVM models that report increased EC proliferation,[25] increased EC footprint,[18,26,27] or both.[28] Increased EC density and decreased EBMSs along Rbpj$^{i\Delta EC}$ vessels are likely related to these initial cellular abnormalities, with impaired EC shape, EC organization, and vessel regression contributing to AV connections being “stalled” in an un-remodeled, wide-diameter state.

We found a role for RBPJ in maintaining directional polarity and focal adhesion properties and in regulating directed cell movement in brain ECs. Our data suggest Rbpj$^{i\Delta EC}$ ECs cannot polarize along the length of an AV connection, and that increased focal adhesion structures may lead to excessive substrate adhesion and reduced EC migration, collectively contributing to impaired directional regression. Our data are consistent with reports that focal adhesion sites regulate cell migration by acting as sites for small GTPase activity.[29–31]

We found that endothelial Rbpj regulates small GTPase activity and expression of Apelin signaling molecules in brain ECs. While other reports showed altered small GTPase activity in vascular malformations,[28,32,33] ours is the first to report Apelin signaling as an intermediary between Rbpj and Cdc42 to influence aspects of cerebrovascular development and prevent bAVM. In the bAVM field, activating mutations in *RAS*[34] have spurred interest in understanding whether Ras/MEK/ERK signaling cooperates with other signaling pathways during bAVM. Our data provide a potential mechanistic link between Rbpj signaling and small GTPase activation in bAVM. Our findings show increased expression of *Spp1/SPP1*, which encodes the extracellular matrix-associated protein Osteopontin, and *Adm/ADM*, which encodes a small GTPase regulatory protein. Consistent with this, *SPP1* and *ADM* expression was upregulated in single cell RNA-Seq data from human bAVM nidus[35], and ADM expression was found in ECs from human aneurysm and bAVM samples.[36] Increased levels of ADM in HHT patient serum and skin telangiectasias suggest ADM as a potential HHT biomarker[37]; however, causal HHT mutations in *Eng* or *Acvrl1* did not alter Adm expression in blood vessels or brain tissue.[38]

Endothelial Rbpj deficiency led to increased expression of *Apelin*, which encodes a ligand for GPCR signaling and promotes coupling to G protein subunits.[21] Consistent with this, Notch regulates Apelin signaling in angiogenic ECs in zebrafish.[24] We identified 12 genes involved in Apelin signaling as direct Rbpj targets (Table S6) and occupancy sites for *Gnai1*

and *Gnaq*, suggesting that Rbpj may regulate GPCR mediated signaling, including small GTPase activity, via Apelin/Apj. Recently, Apelin expression was reported in ECs from infantile hemangioma (IH), a human vascular anomaly, and blockade of Apelin signaling via Aplnr/Apj antagonism suppressed angiogenic tumor formation in an IH mouse model.[39] Our data identify Rbpj as a regulator of *Apelin* and offer potential for pharmacological treatments for bAVM patients with perturbations to Apelin signaling.

Supplementary Material

Refer to Web version on PubMed Central for supplementary material.

Acknowledgements

We thank: LC Sciences (RNA sequencing/analysis); CD Genomics (ChIP sequencing/analysis); Ohio University (OU) IACUC and Laboratory for Animal Research (animal care); OU Neuroscience Program (confocal microscope); OU Histology Core (cryostat); Michelle Pate, OU Flow Cytometry Core (FACS); Dishari Mukherjee (Graphical Abstract).

Sources of funding

This research was supported by OU Honors Tutorial College Research Apprenticeship, Summer Neuroscience Undergraduate Research Fellowship to B.W.; OU Heritage College of Osteopathic Medicine Research and Scholarly Advancement Fellowship to I.P.; OU College of Arts & Sciences, OU Research Council grant 17-40, The Aneurysm and AVM Foundation grant UT 22563, and NIH/NINDS grant R15 NS111376 to C.M.N.

Non-standard Abbreviations and Acronyms

Aplnr/Apj	Apelin receptor
AV	Arteriovenous
bAVM	Brain arteriovenous malformation
Cdc42	Cell division cycle 42
EC	Endothelial cell
GAP	GTPase activator protein
GDI	Guanosine nucleotide dissociation inhibitor
GEF	Guanine nucleotide exchange factor
GPCR	G protein-coupled receptor
GTPase	Guanosine triphosphate hydrolase
P	Postnatal day
Rbpj	Recombination signal-binding protein for immunoglobulin Jκ regions
Rbpj$^{i\Delta EC}$	Inducible deletion of Rbpj from endothelial cells

References

1. Cuervo H, Nielsen CM, Simonetto DA, Ferrell L, Shah VH, Wang RA. Endothelial notch signaling is essential to prevent hepatic vascular malformations in mice. Hepatology. 2016;64:1302–1316. doi: 10.1002/hep.28713 [PubMed: 27362333]
2. Krebs LT, Shutter JR, Tanigaki K, Honjo T, Stark KL, Gridley T. Haploinsufficient lethality and formation of arteriovenous malformations in Notch pathway mutants. Genes Dev. 2004;18:2469–2473. doi: 10.1101/gad.1239204 [PubMed: 15466160]
3. Diaz-Trelles R, Scimia MC, Bushway P, Tran D, Monosov A, Monosov E, Peterson K, Rentschler S, Cabrales P, Ruiz-Lozano P, et al. Notch-independent RBPJ controls angiogenesis in the adult heart. Nat Commun. 2016;7:12088. doi: 10.1038/ncomms12088 [PubMed: 27357444]
4. Dieguez-Hurtado R, Kato K, Giaimo BD, Nieminen-Kelha M, Arf H, Ferrante F, Bartkuhn M, Zimmermann T, Bixel MG, Eilken HM, et al. Loss of the transcription factor RBPJ induces disease-promoting properties in brain pericytes. Nat Commun. 2019;10:2817. doi: 10.1038/s41467-019-10643-w [PubMed: 31249304]
5. Murphy PA, Lam MT, Wu X, Kim TN, Vartanian SM, Bollen AW, Carlson TR, Wang RA. Endothelial Notch4 signaling induces hallmarks of brain arteriovenous malformations in mice. Proc Natl Acad Sci U S A. 2008;105:10901–10906. doi: 10.1073/pnas.0802743105 [PubMed: 18667694]
6. Nielsen CM, Cuervo H, Ding VW, Kong Y, Huang EJ, Wang RA. Deletion of Rbpj from postnatal endothelium leads to abnormal arteriovenous shunting in mice. Development. 2014;141:3782–3792. doi: 10.1242/dev.108951 [PubMed: 25209249]
7. Larrivee B, Prahst C, Gordon E, del Toro R, Mathivet T, Duarte A, Simons M, Eichmann A. ALK1 signaling inhibits angiogenesis by cooperating with the Notch pathway. Dev Cell. 2012;22:489–500. doi: 10.1016/j.devcel.2012.02.005 [PubMed: 22421041]
8. Yao Y, Yao J, Radparvar M, Blazquez-Medela AM, Guihard PJ, Jumabay M, Bostrom KI. Reducing Jagged 1 and 2 levels prevents cerebral arteriovenous malformations in matrix Gla protein deficiency. Proc Natl Acad Sci U S A. 2013;110:19071–19076. doi: 10.1073/pnas.1310905110 [PubMed: 24191040]
9. Hill-Felberg S, Wu HH, Toms SA, Dehdashti AR. Notch receptor expression in human brain arteriovenous malformations. J Cell Mol Med. 2015;19:1986–1993. doi: 10.1111/jcmm.12580 [PubMed: 25846406]
10. Murphy PA, Lu G, Shiah S, Bollen AW, Wang RA. Endothelial Notch signaling is upregulated in human brain arteriovenous malformations and a mouse model of the disease. Lab Invest. 2009;89:971–982. doi: 10.1038/labinvest.2009.62 [PubMed: 19546852]
11. ZhuGe Q, Zhong M, Zheng W, Yang GY, Mao X, Xie L, Chen G, Chen Y, Lawton MT, Young WL, et al. Notch-1 signalling is activated in brain arteriovenous malformations in humans. Brain. 2009;132:3231–3241. doi: 10.1093/brain/awp246 [PubMed: 19812212]
12. Delev D, Pavlova A, Grote A, Bostrom A, Hollig A, Schramm J, Fimmers R, Oldenburg J, Simon M. NOTCH4 gene polymorphisms as potential risk factors for brain arteriovenous malformation development and hemorrhagic presentation. J Neurosurg. 2017;126:1552–1559. doi: 10.3171/2016.3.JNS151731 [PubMed: 27231971]
13. Tzima E. Role of small GTPases in endothelial cytoskeletal dynamics and the shear stress response. Circ Res. 2006;98:176–185. doi: 10.1161/01.RES.0000200162.94463.d7 [PubMed: 16456110]
14. Kidoya H, Ueno M, Yamada Y, Mochizuki N, Nakata M, Yano T, Fujii R, Takakura N. Spatial and temporal role of the apelin/APJ system in the caliber size regulation of blood vessels during angiogenesis. EMBO J. 2008;27:522–534. doi: 10.1038/sj.emboj.7601982 [PubMed: 18200044]
15. Percie du Sert N, Hurst V, Ahluwalia A, Alam S, Avey MT, Baker M, Browne WJ, Clark A, Cuthill IC, Dirnagl U, et al. The ARRIVE guidelines 2.0: Updated guidelines for reporting animal research. PLoS Biol. 2020;18:e3000410. doi: 10.1371/journal.pbio.3000410 [PubMed: 32663219]
16. Chapman AD, Selhorst S, LaComb J, LeDantec-Boswell A, Wohl TR, Adhicary S, Nielsen CM. Endothelial Rbpj Is Required for Cerebellar Morphogenesis and Motor Control in the Early Postnatal Mouse Brain. Cerebellum. 2022. doi: 10.1007/s12311-022-01429-w

17. Selhorst S, Nakisli S, Kandalai S, Adhicary S, Nielsen CM. Pathological pericyte expansion and impaired endothelial cell-pericyte communication in endothelial Rbpj deficient brain arteriovenous malformation. Front Hum Neurosci. 2022;16:974033. doi: 10.3389/fnhum.2022.974033 [PubMed: 36147294]

18. Murphy PA, Kim TN, Huang L, Nielsen CM, Lawton MT, Adams RH, Schaffer CB, Wang RA. Constitutively active Notch4 receptor elicits brain arteriovenous malformations through enlargement of capillary-like vessels. Proc Natl Acad Sci U S A. 2014;111:18007–18012. doi: 10.1073/pnas.1415316111 [PubMed: 25468970]

19. Brown WR. A review of string vessels or collapsed, empty basement membrane tubes. J Alzheimers Dis. 2010;21:725–739. doi: 10.3233/JAD-2010-100219 [PubMed: 20634580]

20. Spindler V, Schlegel N, Waschke J. Role of GTPases in control of microvascular permeability. Cardiovasc Res. 2010;87:243–253. doi: 10.1093/cvr/cvq086 [PubMed: 20299335]

21. Masri B, Morin N, Pedebernade L, Knibiehler B, Audigier Y. The apelin receptor is coupled to Gi1 or Gi2 protein and is differentially desensitized by apelin fragments. J Biol Chem. 2006;281:18317–18326. doi: 10.1074/jbc.M600606200 [PubMed: 16679320]

22. Huang L, Bichsel C, Norris AL, Thorpe J, Pevsner J, Alexandrescu S, Pinto A, Zurakowski D, Kleiman RJ, Sahin M, et al. Endothelial GNAQ p.R183Q Increases ANGPT2 (Angiopoietin-2) and Drives Formation of Enlarged Blood Vessels. Arterioscler Thromb Vasc Biol. 2022;42:e27–e43. doi: 10.1161/ATVBAHA.121.316651 [PubMed: 34670408]

23. Kang Y, Kim J, Anderson JP, Wu J, Gleim SR, Kundu RK, McLean DL, Kim JD, Park H, Jin SW, et al. Apelin-APJ signaling is a critical regulator of endothelial MEF2 activation in cardiovascular development. Circ Res. 2013;113:22–31. doi: 10.1161/CIRCRESAHA.113.301324 [PubMed: 23603510]

24. Kwon HB, Wang S, Helker CS, Rasouli SJ, Maischein HM, Offermanns S, Herzog W, Stainier DY. In vivo modulation of endothelial polarization by Apelin receptor signalling. Nat Commun. 2016;7:11805. doi: 10.1038/ncomms11805 [PubMed: 27248505]

25. Tual-Chalot S, Mahmoud M, Allinson KR, Redgrave RE, Zhai Z, Oh SP, Fruttiger M, Arthur HM. Endothelial depletion of Acvrl1 in mice leads to arteriovenous malformations associated with reduced endoglin expression. PLoS One. 2014;9:e98646. doi: 10.1371/journal.pone.0098646 [PubMed: 24896812]

26. Crist AM, Lee AR, Patel NR, Westhoff DE, Meadows SM. Vascular deficiency of Smad4 causes arteriovenous malformations: a mouse model of Hereditary Hemorrhagic Telangiectasia. Angiogenesis. 2018;21:363–380. doi: 10.1007/s10456-018-9602-0 [PubMed: 29460088]

27. Murphy PA, Kim TN, Lu G, Bollen AW, Schaffer CB, Wang RA. Notch4 normalization reduces blood vessel size in arteriovenous malformations. Sci Transl Med. 2012;4:117ra118. doi: 10.1126/scitranslmed.3002670

28. Fish JE, Flores Suarez CP, Boudreau E, Herman AM, Gutierrez MC, Gustafson D, DiStefano PV, Cui M, Chen Z, De Ruiz KB, et al. Somatic Gain of KRAS Function in the Endothelium Is Sufficient to Cause Vascular Malformations That Require MEK but Not PI3K Signaling. Circ Res. 2020;127:727–743. doi: 10.1161/CIRCRESAHA.119.316500 [PubMed: 32552404]

29. Mishra YG, Manavathi B. Focal adhesion dynamics in cellular function and disease. Cell Signal. 2021;85:110046. doi: 10.1016/j.cellsig.2021.110046 [PubMed: 34004332]

30. Geiger B, Yamada KM. Molecular architecture and function of matrix adhesions. Cold Spring Harb Perspect Biol. 2011;3. doi: 10.1101/cshperspect.a005033

31. Brown MC, Turner CE. Paxillin: adapting to change. Physiol Rev. 2004;84:1315–1339. doi: 10.1152/physrev.00002.2004 [PubMed: 15383653]

32. Castro M, Lavina B, Ando K, Alvarez-Aznar A, Abu Taha A, Brakebusch C, Dejana E, Betsholtz C, Gaengel K. CDC42 Deletion Elicits Cerebral Vascular Malformations via Increased MEKK3-Dependent KLF4 Expression. Circ Res. 2019;124:1240–1252. doi: 10.1161/CIRCRESAHA.118.314300 [PubMed: 30732528]

33. Li QF, Decker-Rockefeller B, Bajaj A, Pumiglia K. Activation of Ras in the Vascular Endothelium Induces Brain Vascular Malformations and Hemorrhagic Stroke. Cell Rep. 2018;24:2869–2882. doi: 10.1016/j.celrep.2018.08.025 [PubMed: 30208313]

34. Nikolaev SI, Vetiska S, Bonilla X, Boudreau E, Jauhiainen S, Rezai Jahromi B, Khyzha N, DiStefano PV, Suutarinen S, Kiehl TR, et al. Somatic Activating KRAS Mutations in Arteriovenous Malformations of the Brain. N Engl J Med. 2018;378:250–261. doi: 10.1056/NEJMoa1709449 [PubMed: 29298116]

35. Winkler EA, Kim CN, Ross JM, Garcia JH, Gil E, Oh I, Chen LQ, Wu D, Catapano JS, Raygor K, et al. A single-cell atlas of the normal and malformed human brain vasculature. Science. 2022;375:eabi7377. doi: 10.1126/science.abi7377 [PubMed: 35084939]

36. Boscolo E, Pavesi G, Zampieri P, Conconi MT, Calore C, Scienza R, Parnigotto PP, Folin M. Endothelial cells from human cerebral aneurysm and arteriovenous malformation release ET-1 in response to vessel rupture. Int J Mol Med. 2006;18:813–819. [PubMed: 17016610]

37. Iriarte A, Ochoa-Callejero L, Garcia-Sanmartin J, Cerda P, Garrido P, Narro-Iniguez J, Mora-Lujan JM, Jucgla A, Sanchez-Corral MA, Cruellas F, et al. Adrenomedullin as a potential biomarker involved in patients with hereditary hemorrhagic telangiectasia. Eur J Intern Med. 2021;88:89–95. doi: 10.1016/j.ejim.2021.03.039 [PubMed: 33888392]

38. Garcia-Sanmartin J, Narro-Iniguez J, Rodriguez-Barbero A, Martinez A. Endoglin and Activin Receptor-like Kinase 1 (Alk1) Modify Adrenomedullin Expression in an Organ-Specific Manner in Mice. Biology (Basel). 2022;11. doi: 10.3390/biology11030358

39. Chen Q, Ying H, Yu Z, Chang L, Chen Z, Chen J, Chang SJ, Qiu Y, Lin X. Apelin Receptor Can Act as a Specific Marker and Promising Therapeutic Target for Infantile Hemangioma. J Invest Dermatol. 2022. doi: 10.1016/j.jid.2022.09.657

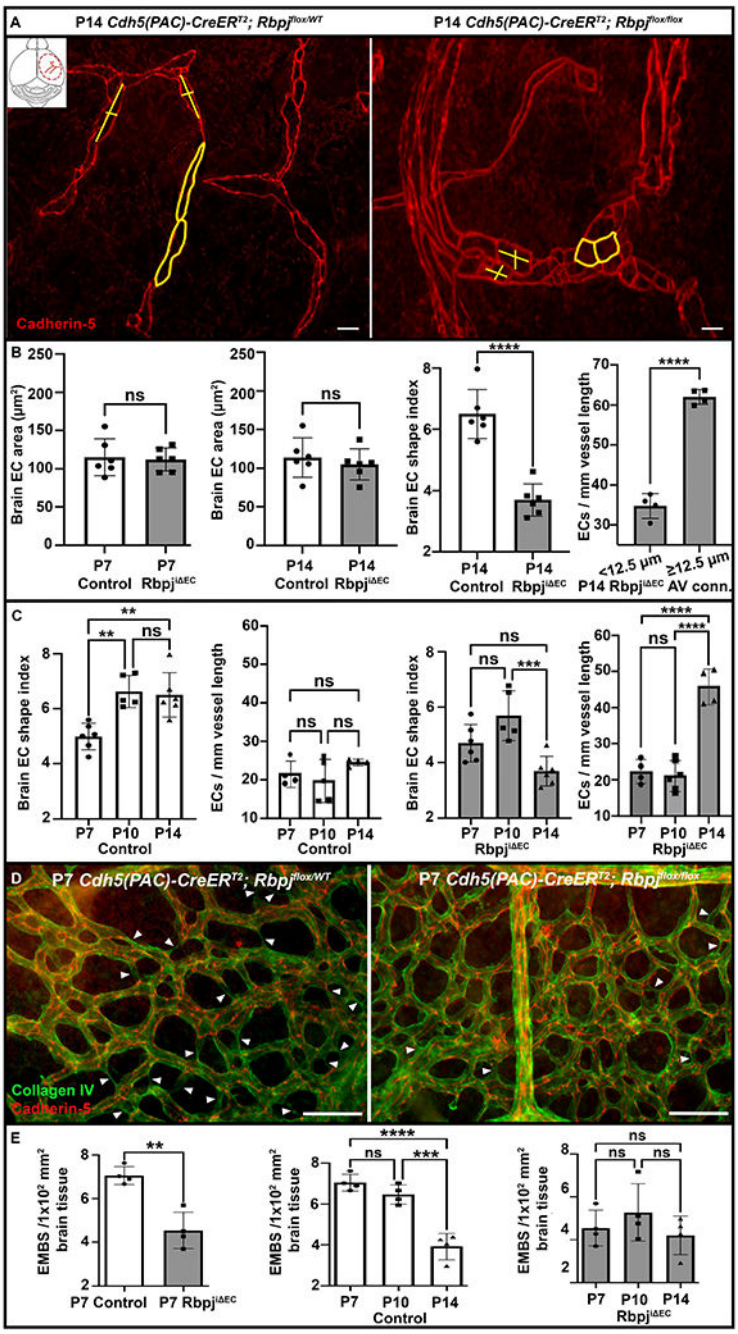

Figure 1. Rbpj$^{i\Delta EC}$ brain ECs exhibited abnormal cellular properties.

(A) Cadherin5(+) ECs were rounded (yellow outlines) by P14 in Rbpj$^{i\Delta EC}$, compared to control. For shape index (yellow lines), length followed direction of flow. a, artery; v, vein. Scale, 10 μm. (B) EC area remained unchanged at P7 (p=0.8100) and P14 (p=0.5201) in Rbpj$^{i\Delta EC}$ mice compared to controls (N=6). EC shape index was reduced in Rbpj$^{i\Delta EC}$ mice by P14 (N=6, p<0.0001). EC density was increased in Rbpj$^{i\Delta EC}$ AV shunts with ≥12.5 μm diameter compared to AV connections with <12.5 μm diameter (p<0.0001). (C) Control EC shape index increased from P7 – P10 (p=0.0024) and remained unchanged from P10 – P14

(p=0.9473). EC density did not change from P7 – P10 – P14 in control mice (p=0.2839). Brain EC shape index remained unchanged in Rbpj$^{i\Delta EC}$ mice from P7 – P10 (p=0.0811) and decreased from P10 to P14 (p=0.0009). Brain EC density increased from P7/P10 – P14 in Rbpj$^{i\Delta EC}$ mice (p<0.0001). (D) Fewer Collagen IV(+)/Cadherin5(−) EBMS structures (arrowheads) were observed in P7 Rbpj$^{i\Delta EC}$ brain vasculature than controls. Collagen IV, green. Cadherin5, red. Scale, 100 μm. Quantified in (E), (p=0.0047). (E) Control mice had overall decrease in EBMS number (p<0.0001), with no change from P7 – P10 and decrease from P10 – P14 (p=0.0001). Rbpj$^{i\Delta EC}$ showed no change in EBMS dynamics (p=0.3837).

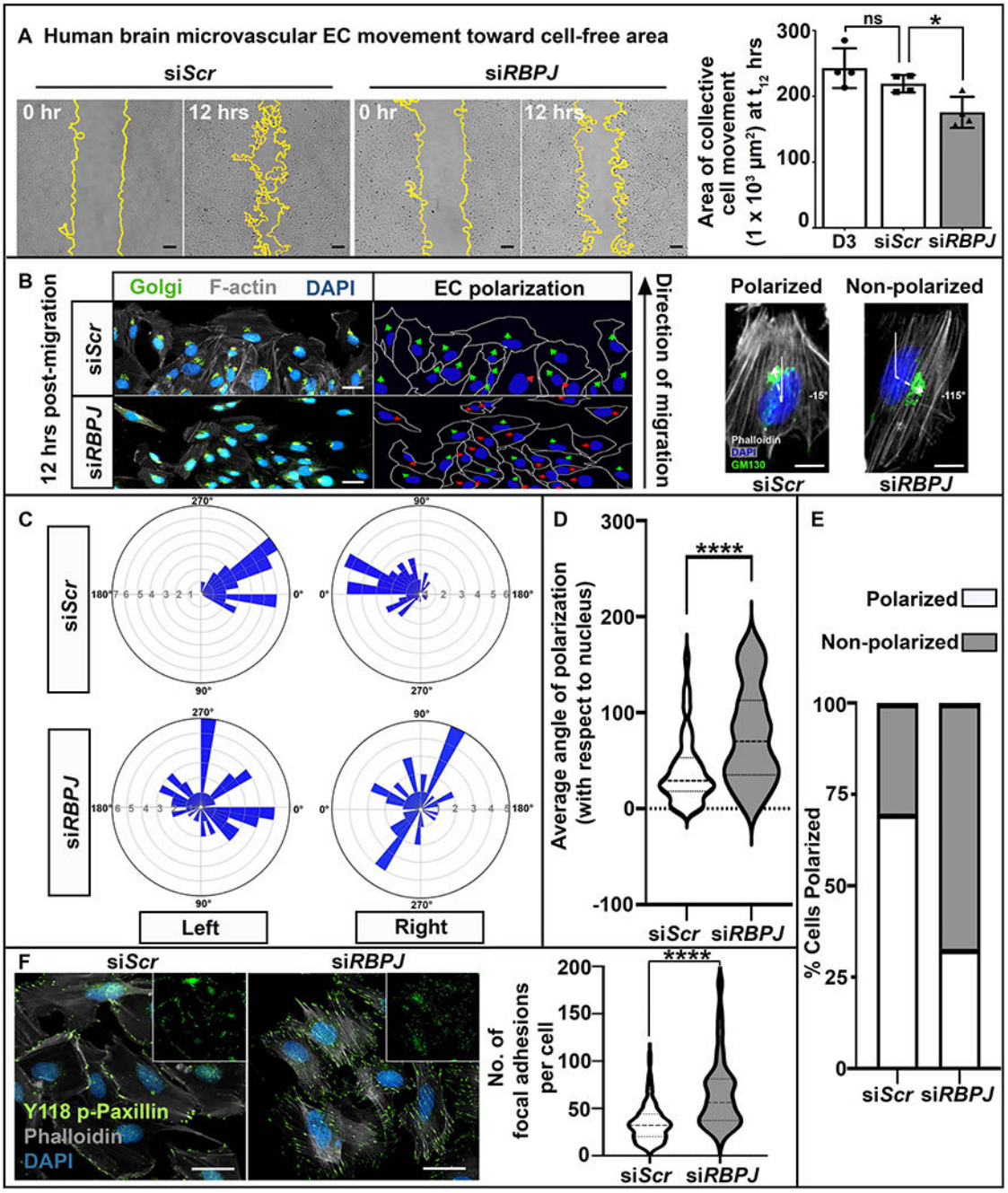

Figure 2. RBPJ knockdown led to impaired migration, directionality, and polarity of brain ECs.

(A) si*Scr* control and *siRBPJ* human microvessel ECs at 0 hr and 12 hr timepoints. Yellow outlines, cell-free areas. Scale, 100µm. si*RBPJ* ECs had reduced cell movement compared to si*Scr* and non-transfected cells. (B) *siScr* control and si*RBPJ* ECs immunolabeled for Golgi apparatus (GM130, green), F-actin (Phalloidin, grey), and nuclei (DAPI, blue) 12 hrs post-migration. Scale, 20 µm. Schematic indicates directionality with green (polarized) and red (non-polarized) arrows. High-magnification of polarized si*Scr* (−15°) and non-polarized si*RBPJ* (−115°) ECs. (C) Rose plots show frequency of Golgi-nuclear angles in si*Scr* and

si*RBPJ* ECs. Gap represents cell-free area. (D) Average angle of polarization increased in si*RBPJ* ECs compared to si*Scr*. Plot shows 1st, 3rd quartiles and median (N=~100 cells, p<0.0001). (E) Percentage of polarized ECs decreased in si*RBPJ* compared to si*Scr*. (F) Number of phospho-paxillin(+) focal adhesions (green) increased in si*RBPJ* compared to si*Scr* (N=~50, p<0.0001). F-actin (Phalloidin, grey) and nuclei (DAPI, blue). Scale, 20 μm.

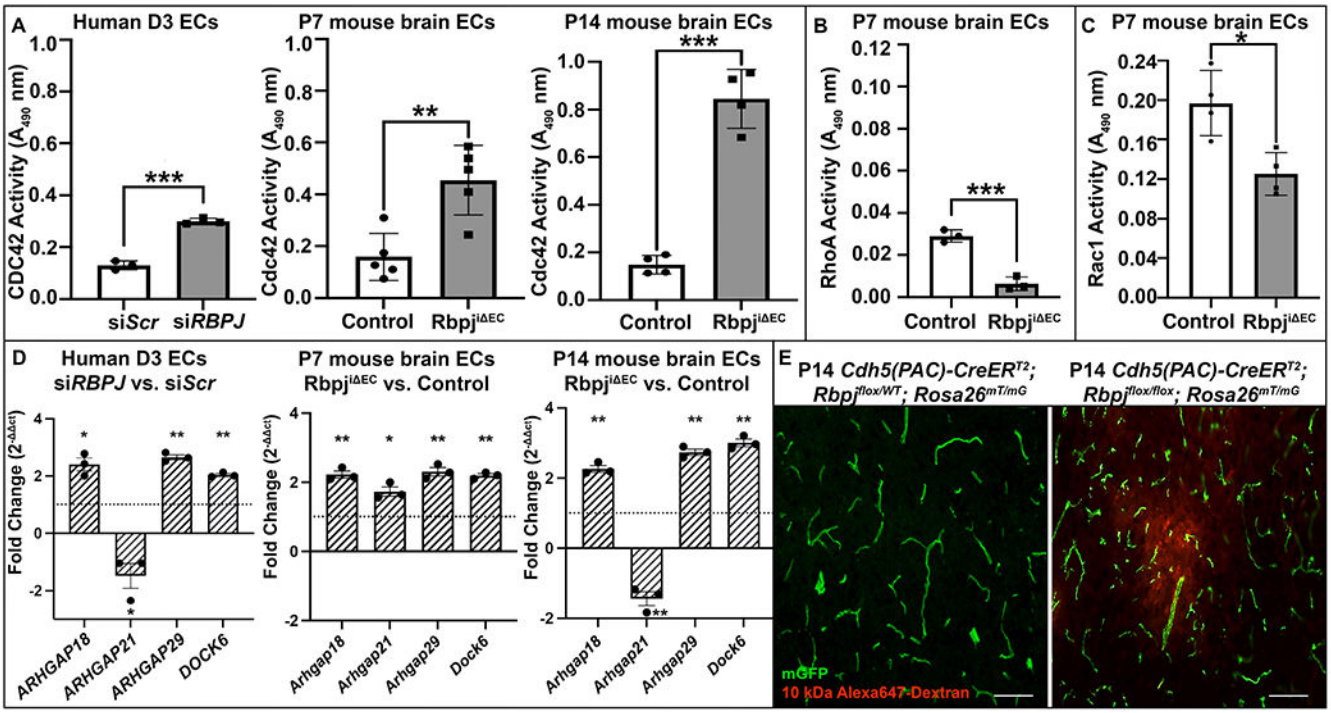

Figure 3. Dysregulated GAP/GEF expression, small GTPase activity, and vascular permeability in Rbpj$^{i\Delta EC}$ mice.

Cdc42 activity was increased in (A) si*RBPJ* human brain ECs (N=3, p=0.0003) compared to si*Scr* and in P7 (N=5, p=0.0046) and P14 (N=4, p=0.0007) Rbpj$^{i\Delta EC}$ ECs compared to controls. (B-C) RhoA (N=3, p=0.0009) and Rac1 (N=4, p=0.0144) showed increased activity in P7 Rbpj$^{i\Delta EC}$ ECs compared to controls (D) Relative gene expression of *ARHGAP18* (P=0.0242), *ARHGAP29* (P=0.0026), and *DOCK6* (P=0.0019) was increased, while *ARHGAP21* (P=0.0291) was decreased, in si*RBPJ* ECs compared to si*Scr* (N=3). Dotted line indicates no change. Relative gene expression of *Arhgap18* (P=0.0068), *Arhgap21* (P=0.0340), *Arhgap29* (P=0.0082), and *Dock6* (P=0.0019) was increased at P7 in Rbpj$^{i\Delta EC}$ mice (N=3). Relative gene expression of *Arhgap18* (P=0.0055), *Arhgap29* (P=0.0028), and *Dock6* (P=0.0027) was increased, while *Arhgap21* (P=0.0069) was decreased, at P14 in Rbpj$^{i\Delta EC}$ mice (N=3). (E) Ten kDa dextran (red) was extravasated from mGFP(+) vasculature in Rbpj$^{i\Delta EC}$ but not controls. Scale, 50 μm.

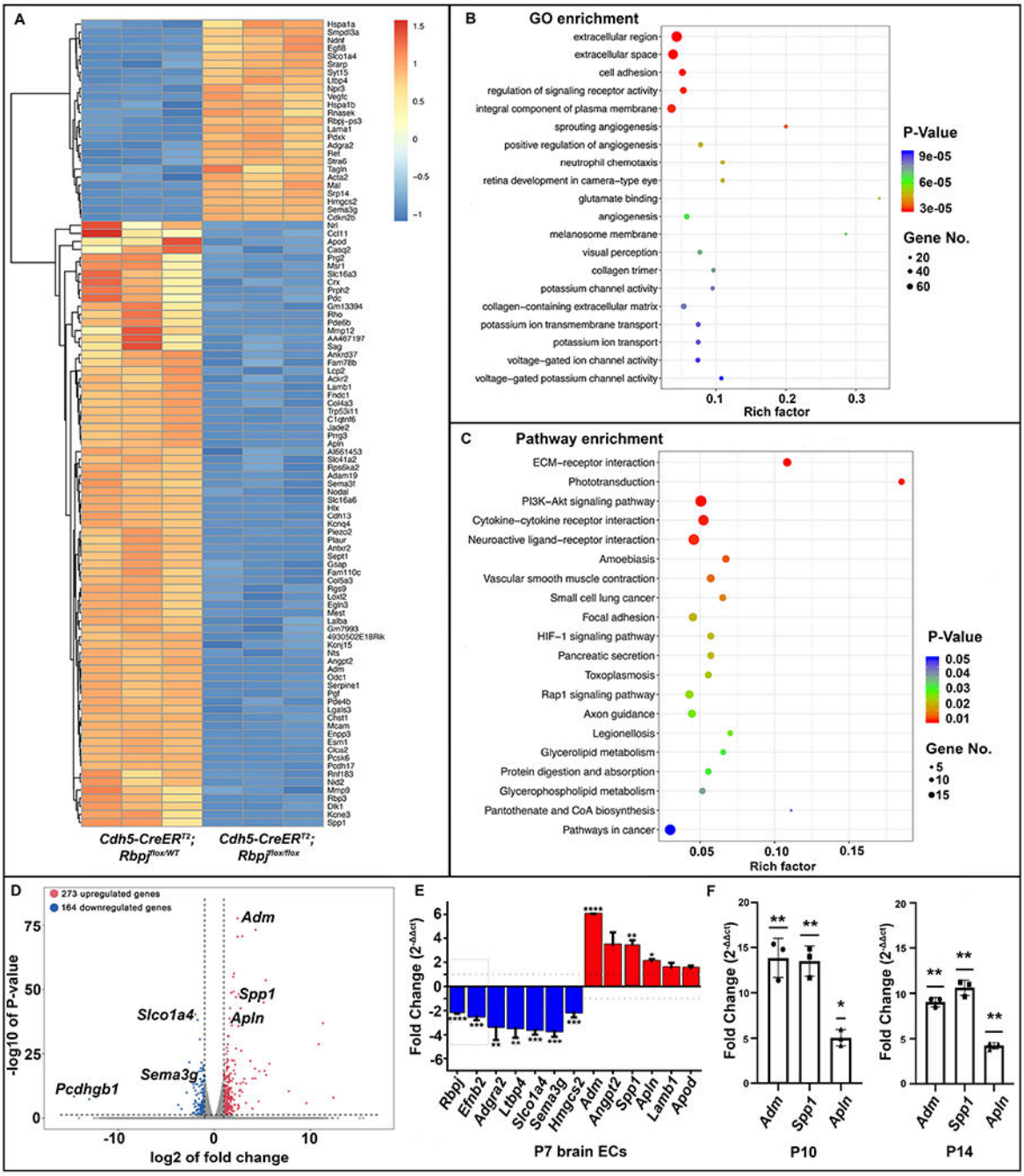

Figure 4. RNA sequencing analysis identified differentially expressed small GTPase-regulatory genes in Rbpj$^{i\Delta EC}$ versus control.

(A) Heat map of DEGs in technical replicates. Red and blue indicate increasingly upregulated and downregulated expression, respectively. (B) Scatter plot shows gene ontology (GO) (Y-axis) enrichment analysis. X-axis = number of DEGs/total number of genes, within one GO term. Gene number = number of genes within GO term. Significance increases from blue to red. (C) Scatter plot depicting KEGG pathway (Y-axis) enrichment analysis. X-axis = number of DEGs in KEGG pathway/total number of genes annotated in KEGG pathway. Significance increases from blue to red. (D) Volcano plot shows select

DEGs up- (red) or down-(blue) regulated. (E) Relative gene expression ($Rbpj^{i\Delta EC}$ versus Control) from P7 ECs. Upregulated genes (red); downregulated genes (blue). Dotted lines indicate no change in gene expression (N>3 for triplicates of 3 independent experiments). (F) *Adm*, *Spp1* and *Apln* expression levels were increased at P10 (P=0.0105) and P14 (P=0.0028) in $Rbpj^{i\Delta EC}$ compared to controls (N>3 for each of 3 replicates).

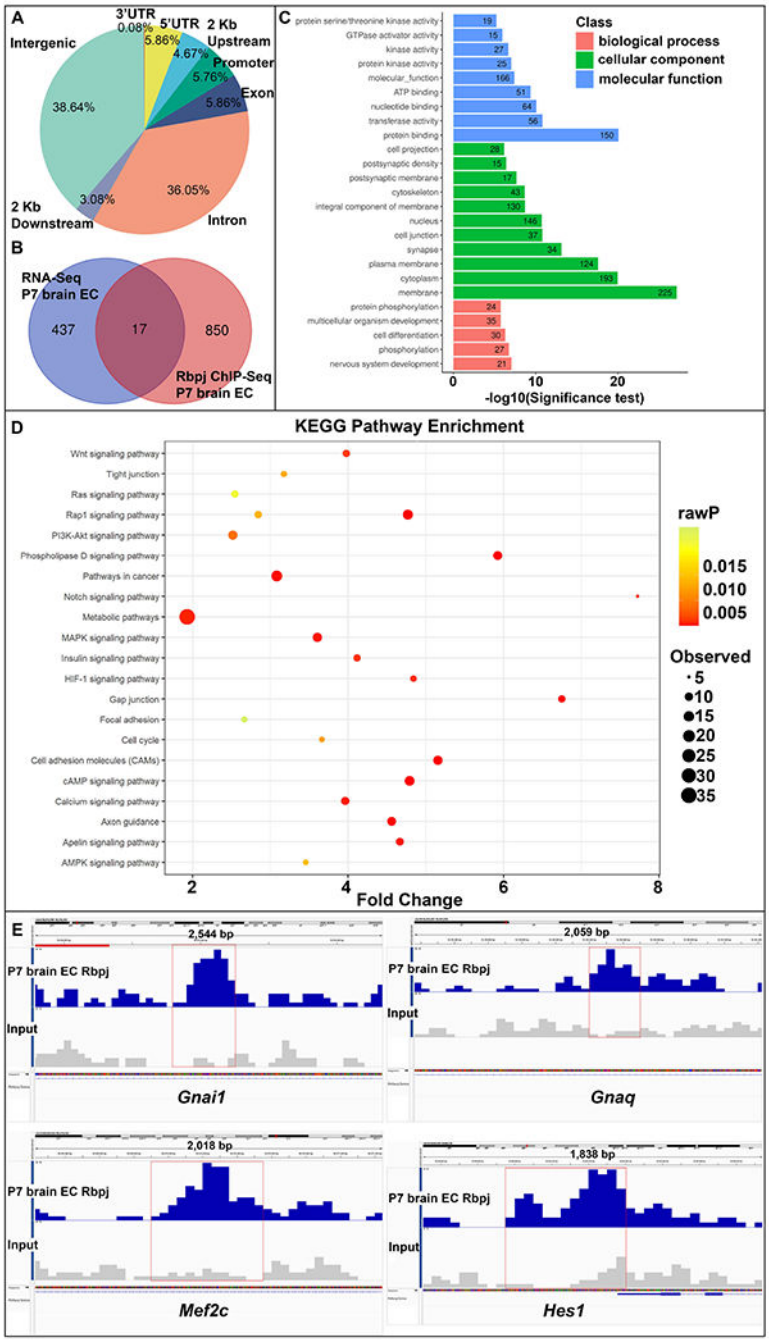

Figure 5. ChIP sequencing analysis identified chromatin loci occupied by Rbpj.

(A) Genomic distribution of Rbpj binding, including 3' untranslated regions (UTR), 5' UTR, 2 kb upstream, promoter, exon, intron, 2 kb downstream, and intergenic regions. (B) Seventeen genes were identified as DEGs via RNA-Seq and Rbpj targets via ChIP-Seq. (C) GO enrichment analysis shows gene categories identified as Rbpj binding targets. (D) Scatter plot depicts KEGG pathway (Y-axis) enrichment analysis. X-axis = ratio of DEGs in KEGG pathway/total number of genes annotated in KEGG pathway. Significance increases

from green to red. (E) Rbpj enrichment peaks around *Gnai1*, *Gnaq*, *Mef2c*, *Hes1*, in P7 brain ECs.

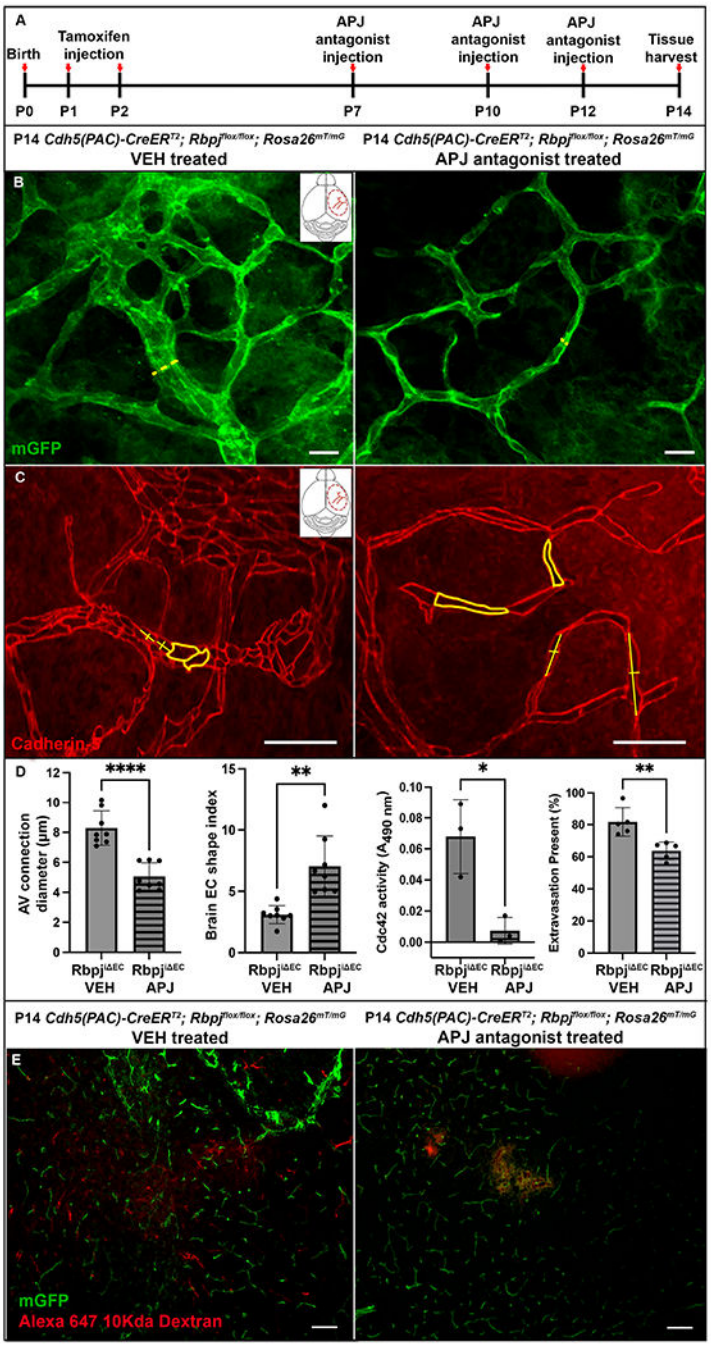

Figure 6. Blockade of Apelin/APJ signaling restored brain AV connection diameter, EC shape index, and Cdc42 activity in Rbpj$^{i\Delta EC}$ mice.

(A) Experimental timeline. (B) Rbpj$^{i\Delta EC}$ mice treated with VEH developed AV shunts (mGFP+ ECs). Rbpj$^{i\Delta EC}$ mice treated with Apj antagonist retained capillary network by P14. Yellow lines, AV diameter measurement. Scale, 100 μm. (C) Cadherin5(+) (red) ECs were rounded in P14 VEH-treated mice; ECs were elongated in Apj antagonist-treated mice. Outlines, area; lines, shape index. Scale, 50 μm. (D) AV diameter was reduced in Apj antagonist-treated mice compared to VEH-treated ($p<0.0001$). EC shape index was increased in Apj antagonist-treated mice compared to VEH-treated ($p=0.0023$). Cdc42

activity was decreased in Apj antagonist-treated mice compared to VEH-treated (p=0.0361). Dextran extravasation was decreased in Apj antagonist-treated mice compared to VEH-treated (p=0.007). (E) Alexa647-Dextran (10 kDa) extravasation (red) was decreased in Apj antagonist-treated tissue compared to VEH-treated. Scale, 50 μm.